Progress In Electromagnetics Research B, Vol. 61, 43–54, 2014

Automatic Recognition of ISAR Images of Multiple Targets and ATR Results

Sang-Hong Park*

Abstract—Inverse synthetic aperture radar (ISAR) imaging is an effective method to identify unknown targets regardless of weather and illumination conditions. Research results published regarding this topic have focused mainly on imaging and automatic target recognition (ATR) of single targets. However, targets generally fly in formation, so the applicability of ISAR images to ATR of multiple targets must be studied. This paper proposes an ATR procedure for targets flying in formation. ATR accuracy derived using five targets composed of point scatterers and the measured radar signal of a Boeing 747 aircraft was as high as that of the solo flight in terms of SNR and the size of the training database; this result shows that ISAR is an adequate tool for ATR even if an image is contaminated by radar reflections from neighboring targets.

1. INTRODUCTION

An inverse synthetic aperture radar (ISAR) image [1–7] represents the two-dimensional radar cross-section (RCS) distribution of a target. An ISAR image of the target can be generated by synthesizing compressed radar signals at various observation angles. Due to its applicability regardless of weather and illumination conditions, it is used in many military applications such as classification of non-cooperative aircraft, and battlefield awareness [8, 9].

The main impediment to ISAR imaging is to identify flying targets that are moving in formation; this is because each target may have complicated motion components, which can degrade the quality of its ISAR image. Efficient algorithms such as range-Doppler [10] and time frequency analysis [11] were proposed to image a single target, but when multiple targets occur in a single radar beam, imaging each target separately is a difficult task. To solve this problem, [12] proposed a segmentation method that can separate ISAR images of aircraft flying in formation; in this method, coarse alignment proposed in [13] was improved by using a combination of a polynomial and Gaussian basis functions, and segmentation was improved using an image processing technique.

However, the ISAR image segmented by the segmentation method is a mere projection of the target and can be contaminated by radar signals reflected from neighboring targets. For this image to be useful, the segmented image must be identified by the automatic target recognition (ATR) technique and its accuracy must be evaluated. Many approaches to image stationary targets or those engaged in solo flight have been presented and their ATR accuracy have been published [14]. However, little research on segmenting ISAR images of targets flying in formation has been reported due to the sensitive military applications of this topic.

This paper proposes a procedure for ATR of an ISAR image by fusing a method to segment the ISAR image, a scenario-based method to construct the training database, and an efficient polar-mapping classifier [1]. ATR results are presented by using the ISAR images segmented from three targets composed of point scatterers (SCs) and the measured radar signal from a Boeing 747 aircraft. ATR accuracy degraded $< 1\%$ in spite of the image quality degradation; this result demonstrates that

Received 8 July 2014, Accepted 21 August 2014, Scheduled 11 September 2014

* Corresponding author: Sang-Hong Park (radar@pknu.ac.kr).
The author is with the Department of Electronic Engineering, Pukyong National University, Busan, Korea.

a 2D ISAR image is appropriate for ATR even when each image is contaminated by radar reflections from neighboring targets.

2. PRINCIPLES AND SUMMARY OF THE CLASSIFICATION METHOD

2.1. Signal Modeling and Imaging Algorithm

For the radar signal, we assume the monostatic chirp radar signal that is widely used for high resolution radar imaging. The transmitted chirp signal is given by [1]

$$r(t) = A_0 e^{j2\pi\left(f_0 t + \frac{Bt^2}{2\tau}\right)} \times \text{rect}\left(\frac{t}{\tau}\right), \tag{1}$$

where $r(t)$ is a transmitted signal at time t, A_0 its amplitude, f_0 the start frequency, B the bandwidth, τ the pulse duration, and rect = 1 for $t - \tau/2 \le t \le t + \tau/2$ and 0 otherwise [1]. For a single target composed of L SCs at aspect angle θ, the received reflected signal is [1]

$$g(\theta, t) = \sum_{l=1}^{L} A_l e^{j2\pi\left(f_0(t-d_{l,\theta}) + \frac{B(t-d_{l,\theta})^2}{2\tau}\right)} \times \text{rect}\left(\frac{t - d_{l,\theta}}{\tau}\right), \tag{2}$$

where A_l is the amplitude of scattering center l and $d_{l,\theta}$ the time delay between the radar and scattering center l. For K targets flying in formation, (2) is changed to [12]

$$g(\theta, t) = \sum_{k=1}^{K} \sum_{l=1}^{L} A_{k,l} e^{j2\pi\left(f_0(t-d_{k,l,\theta}) + \frac{B(t-d_{k,l,\theta})^2}{2\tau}\right)} \times \text{rect}\left(\frac{t - d_{k,l,\theta}}{\tau}\right), \tag{3}$$

where $A_{k,l}$ and $d_{k,l,\theta}$ correspond to A_l and $d_{l,\theta}$ in (2) for target k. Reflections from neighboring targets interfere with the radar signal returned from each target.

In deriving the whole ISAR image of the multiple targets, the reflected signal is matched-filtered to obtain range profiles (RPs) at each θ. Then RPs are aligned by minimizing the entropy cost function [3–5] defined by

$$H_{G_m, G_{m+1}} = -\sum_{0}^{N-1} \bar{G}(s,n) \ln \bar{G}(s,n), \tag{4}$$

where

$$\bar{G}(s,n) = \frac{|G_m(n)| + |G_{m+1}(n-s)|}{\sum_{0}^{N-1} \left(|G_m(n)| + |G_{m+1}(n-s)|\right)}, \tag{5}$$

$G_m(n)$ and $G_{m+1}(n)$ are RPs m and $m+1$, and N is the total number of range bins. The s that minimizes the 1D entropy is the shift that best aligns RP $m+1$. Then, to remove residual phase errors that range between ± (range bin)/2, the phase error vector that minimizes the following 2D entropy function is found [12]:

$$Ent = -\sum_{i=1}^{M} \sum_{j=1}^{N} \left|\bar{I}(i,j)\right| \ln \left|\bar{I}(i,j)\right|, \tag{6}$$

where

$$\left|\bar{I}(i,j)\right| = \frac{|I(i,j)|^2}{\sum_{m=0}^{M-1} \sum_{n=0}^{N-1} |I(m,n)|^2}, \tag{7}$$

and I is the ISAR image derived from the RPs with RP m multiplied by the mth element of the phase vector. M is the number of RPs and N the number of range bins. Each RP is multiplied by each element of the phase vector, and finally, SCs are separated in the cross-range direction by performing

a fast Fourier transform in each range bin. Because multiple targets are separated in the 2D range-Doppler domain after this step, the ISAR image of each target can be clipped from the whole ISAR image and the clipped image can be enhanced by applying range alignment (RA), phase adjustment (PA) and fast Fourier transform (FFT) in each range bin to the clipped image.

To increase the effectiveness with which the ISAR image of each target is separated, we recently proposed a new method that is composed of a new cost function for RA and a segmentation method [12]. Because constructive and destructive interference among various scatterers of multiple targets can cause range profiles to be highly uncorrelated, the entropy cost function for RA can poorly align range profiles; generally high-valued range bins were aligned in [13]. Therefore, for each range bin to have equal weight in RA, we constructed a binary bulk image of the range profile history and proposed a new cost function [13] which is the sum of all pixels that occur in the following polynomial:

$$f(t) \;=\; \sum_{i=0}^{P} p_i t^i \;+\; \sum_{i=0}^{G} a_i \exp\left(-\left(\frac{t-b_i}{c_i}\right)^2\right), \tag{8}$$

where P is the order of the polynomial, p_i its parameters, $G+1$ the number of Gaussian basis functions, and a_i, b_i, c_i are their parameters. The parameters were found using a combination of the gradient-based method and particle-swarm optimization (PSO) [15]. As the segmentation algorithm, we used the conventional CFAR detector:

$$T(x) = \frac{x - \hat{\mu}_c}{\hat{\sigma}_c}, \tag{9}$$

where x is the amplitude of the test pixel, $\hat{\mu}_c$ the estimated mean of the clutter amplitude, and $\hat{\sigma}_c$ the estimated standard deviation of the clutter amplitude. If $T(x)$ exceeds a threshold, the corresponding binary pixel value is 1; it is 0 otherwise. In setting $T(x)$, if it is too large, the target pixel can be removed and if too small, the clutter can be detected. In our numerous tests, $T(x)$ between 2 and 4 was appropriate. Then, image closing defined as image dilation followed by image erosion was applied to the binary image to fill the target region as follows:

$$C(A, B) = (A \bullet B) \circ B, \tag{10}$$

where C is the closing operation, $\bullet$ the dilation operation, and $\circ$ the erosion operation (details in [12]). The connected set of the binary was clipped and multiplied by the whole ISAR image to segment each target from the ISAR image of the whole set of targets.

2.2. Proposed Classification Procedure

In classifying ISAR images, ISAR images of a test target must exist in the training database. This requirement results in serious computational burden due the infinite number of aspect angles. For this reason, we obtain the training database of the ISAR image by applying a method that is based on flight scenarios of a target (Fig. 1) [1]. Assuming that a target moves at a given velocity in a given direction starting from each point uniformly sampled in the 3D space (training space), the training database is constructed using the ISAR images derived for each flight scenario.

In classification, various classifiers can be used. We use the polar mapping classifier (PMC) which is invariant to variation in the scale and the translation of the ISAR image [16]. This method removes the rotational variance by converting the rotation of the ISAR image to translation in the angular direction by mapping the ISAR image in polar coordinates, then compressing it using principal component analysis. The algorithm makes the final identification by comparing the compressed image to images in a database.

Classification is conducted by fusing the principles mentioned above(Fig. 2). The test targetsfly in formation starting from a random location in the training space (Fig. 1) and the reflected signal is collected using (3). To derive the ISAR image of the whole set of targets, the collected signal is matched-filtered and coarse range alignment is conducted using (8), PSO and the cost function in [12]. Then phase adjustment and cross-range FFT are applied to obtain the ISAR image of the test targets under formation flight.

In segmenting each target, the binary image using (9) is constructed, image closing is conducted on the binary image and finally the connected set of the binary was clipped and multiplied by the whole

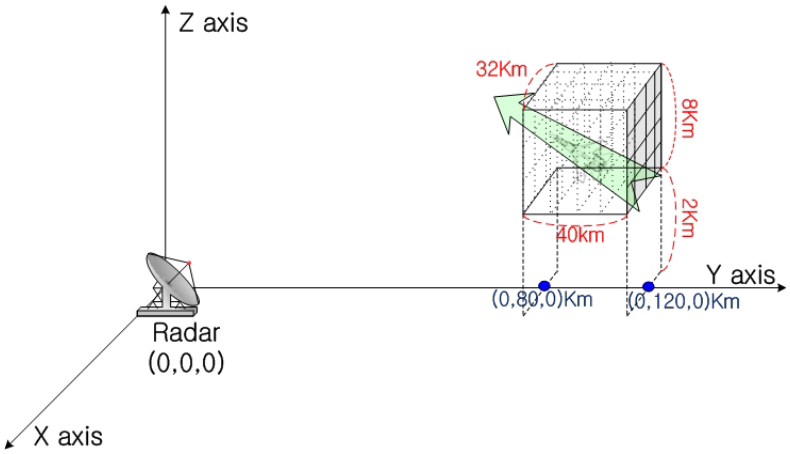

Figure 1. Scenario-based construction method ([−1 −1 0] direction) [1].

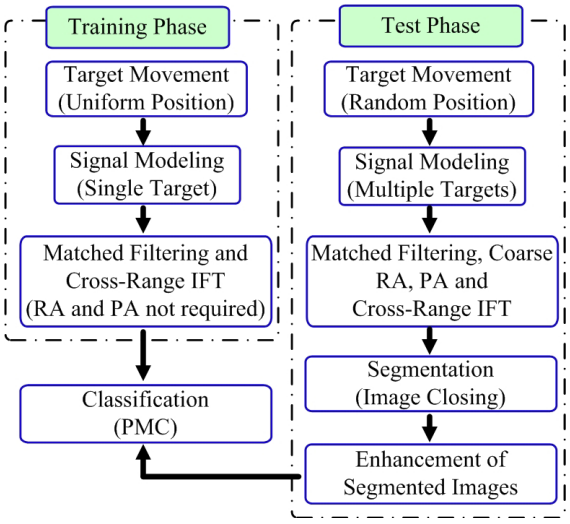

Figure 2. Proposed classification procedure.

ISAR image. The segmented ISAR image is classified by the PMC. Classification accuracyis expressed as the correct classification percentage

$$P_c = \frac{N_c}{N_t} \times 100\%, \tag{11}$$

where N_c is the number of the correct identifications and N_t the number of test sets.

3. SIMULATION RESULTS

3.1. Simulation Results Using the Point Scatterer Model

To demonstrate the effectiveness of the proposed method and to evaluate the ATR accuracy of the segmented ISAR image, simulations were conducted using targets composed of point SCs. The simulation used pulse repetition frequency (PRF) = 2 kHz, center frequency $f_0 = 10.0$ GHz, bandwidth $B = 200$ MHz (0.75-m range resolution). The signal-to-noise ratio was varied to study the effect of noise. The parameters used in PSO were population size = 50, number of generations = 20, $\varphi = 0.5$, and $c_1 = c_2 = 1.49$ (definitions in [3]). Five targets were used for simulation; they were constructed

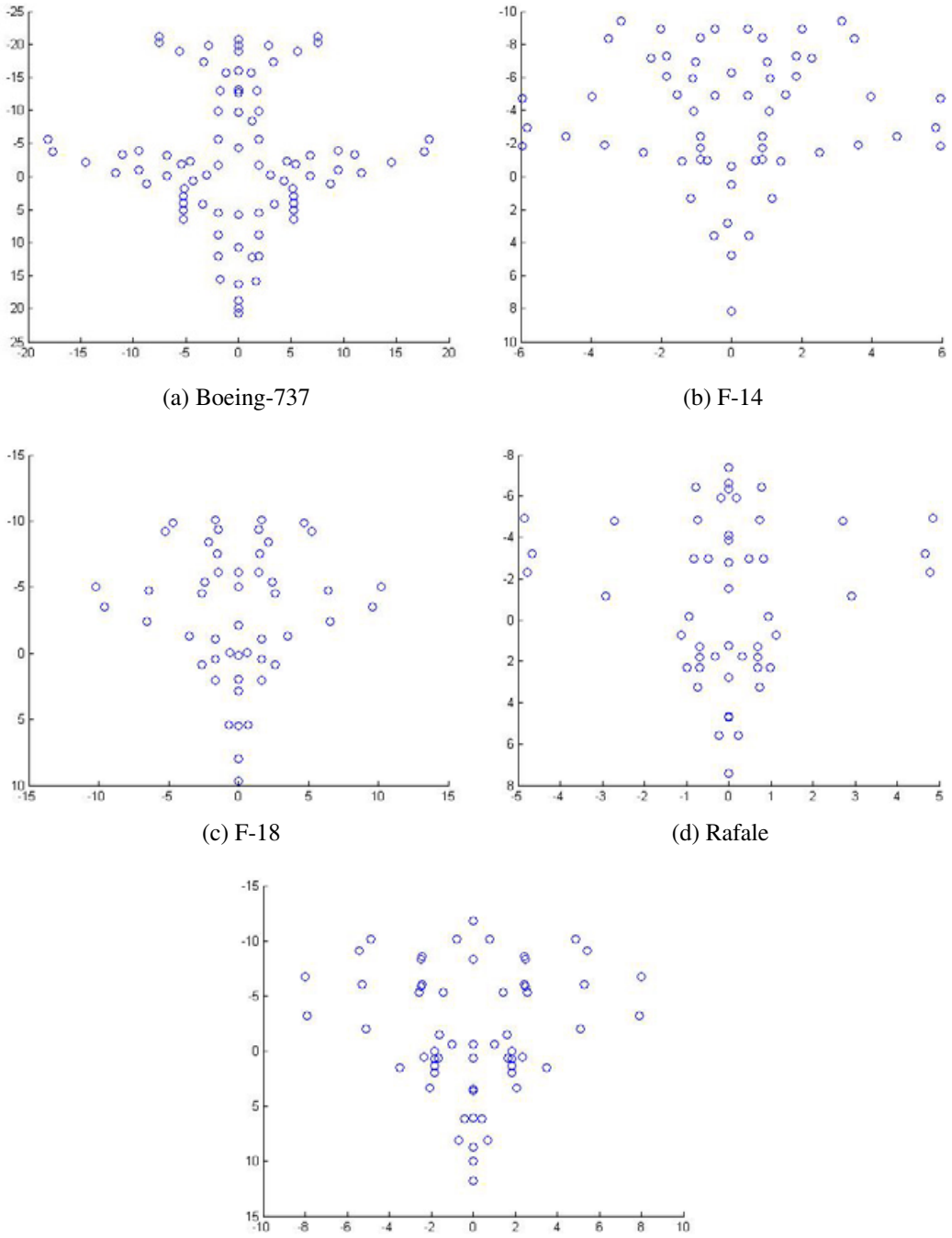

(a) Boeing-737

(b) F-14

(c) F-18

(d) Rafale

(e) Su-35

Figure 3. Scatterer targets used for classification.

using the 3D CAD data of a Boeing 737, an F-14, an F-18, a Rafale, and an Su-35 (Fig. 3). Two separate simulations were performed for each formation flight; one with three identical targets and the other with randomly chosen targets. The relative distances between the centers of the aircraft were 60 m for the Boeing-737, 35 m for the Su-35 and 25 m for the others.

The training database was constructed based on formation flights in two directions, $[-1\ -1\ 0]$ and $[0\ -1\ 0]$ and we assumed that the aircraft flew at $v = 300\,\mathrm{m/s}$. Using $N_g = 5$ which is the number of

grids in each axis, we sampled the space ($-16 \leq x \leq 16$ km, $80 \leq y \leq 120$ km, $2 \leq z \leq 10$ km) with a regular grid yielding $N_g \times N_g \times N_g = 125$ starting points. Then ISAR images were constructed for each flight direction using the given starting points. The aircraft flew until the aspect angle variation was 1.26°, which corresponds to 0.75-m cross-range resolution. RA and PA were not conducted because the motion parameters of the target were known. To reduce the computation time, the received signals were down-sampled to 300 equally-spaced pulses for the Boeing 737 and 128 pulses for the others. Additive white Gaussian noise was added to the reflected signals for various SNRs.

In constructing the test images, 20 simulations were conducted for each target in a given flight direction starting from random positions, yielding $5 \times 20 \times 3 = 300$ test images. Because the motion of the test target was not known, RA and PA were conducted. Three F-14s flying in the [−1 −1 0] direction were properly separated after coarse RA, PA and cross-range FFT (Fig. 4), but each aircraft was blurred due to the mutual interference of the targets. Clearly, each segmented and enhanced target (Fig. 5) was more focused than that in Fig. 4, and as a result, the entropy defined by (5) considerably improved after image enhancement (Table 1).

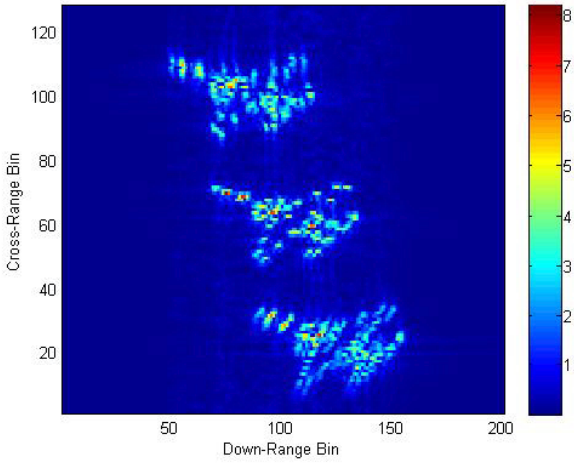

Figure 4. ISAR image of the three F-14s in formation.

Table 1. Entropy comparison of targets in Figures 4 and 5.

Figure	F-14 number		
	1	2	3
4	−6.7211	−6.3517	−6.7255
5	−6.1778	−6.1777	−6.1775

P_c at SNR = 10 dB was very high for the random and the identical targets flying in [−1 −1 0] and [−1 0 0] directions (Tables 2 and 3). Compared with the case of single target classification [1], P_c was degraded by only 1–2%. The Boeing 737 was perfectly classified and the P_cs of the others degraded slightly. P_cs derived using ISAR images were higher by 4–5% than those obtained by 1D RPs [17] because 2D ISAR images represented the characteristics of each target better than did 1D RP. The results in the [−1 0 0] were slightly better than those in the [−1 −1 0] directions, because in the 2D range-Doppler domain the [1 0 0] image was more widely spread than the [−1 −1 0] image.

In simulations to study the effect of SNR variation, segmented ISAR images derived from the formation flight of the identical and the randomly selected targets yielded very good and stable classification results ($94.3 \leq P_c \leq 97.7\%$) for the two flight scenarios (Figs. 6(a), (b)). P_cs of the randomly selected targets degraded by $< 1\%$. Compared with the single-target classification, the P_c degradation was $0.9 \sim 2.4\%$. This result demonstrates the advantage of an ISAR image; even though each individual RP may be contaminated by neighboring targets, information loss in the ISAR image derived by the coherent processing of the RPs was not severe.

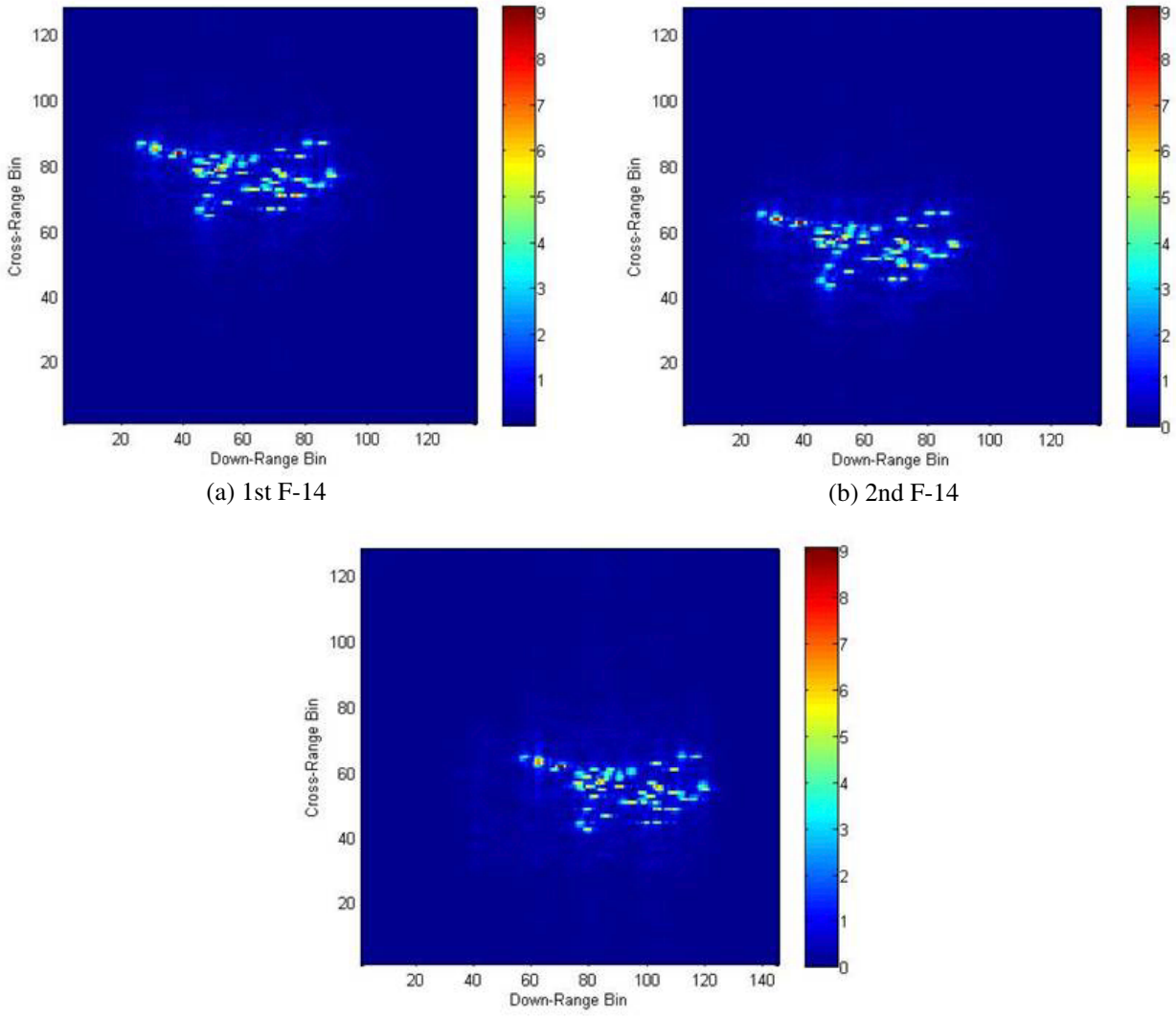

(a) 1st F-14

(b) 2nd F-14

(c) 3rd F-14

Figure 5. Segmented and enhanced ISAR images.

Table 2. Confusion matrices for the flight in $[-1\ -1\ 0]$ direction.

Three identical targets ($P_c = 96.7\%$)					
Actual	Classification				
Class	B737	F14	F18	Rafale	Su35
B737	60	0	0	0	0
F14	0	60	0	0	3
F18	0	2	58	0	0
Rafale	0	4	0	56	0
Su35	0	1	3	0	56

Three random targets ($P_c = 96.0\ \%$)					
Actual	Classification				
Class	B737	F14	F18	Rafale	Su35
B737	64	0	0	0	0
F14	0	60	1	2	0
F18	0	2	52	0	0
Rafale	0	2	0	54	1
Su35	0	0	3	1	58

Segmented ISAR images were insensitive to the reduction of the training vector size (Fig. 7). N_g was changed from 5 to 2 at SNR = 10 dB, yielding correspondingly reduced numbers of training images $N_{tr} = N_g^3$ per target. As in Fig. 6, P_cs of random targets slightly degraded ($0.3 \sim 1\%$). In the two

Table 3. Confusion matrices for the flight in [−1 0 0] direction.

Three identical targets ($P_c = 97.7\%$)

Actual Class	Classification				
	B737	F14	F18	Rafale	Su35
B737	60	0	0	0	0
F14	0	60	0	0	3
F18	0	1	58	0	1
Rafale	0	0	1	58	1
Su35	0	0	1	2	57

Three random targets ($P_c = 96.3\ \%$)

Actual Class	Classification				
	B737	F14	F18	Rafale	Su35
B737	57	0	0	0	0
F14	0	56	1	1	0
F18	0	1	61	1	1
Rafale	0	0	1	55	1
Su35	0	1	1	2	60

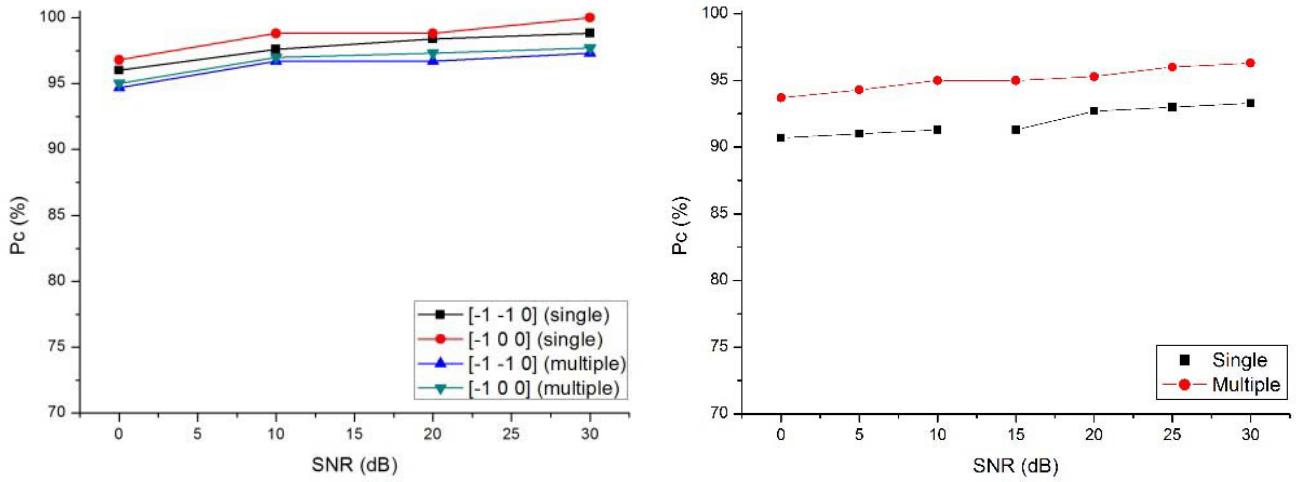

(a) Identical targets

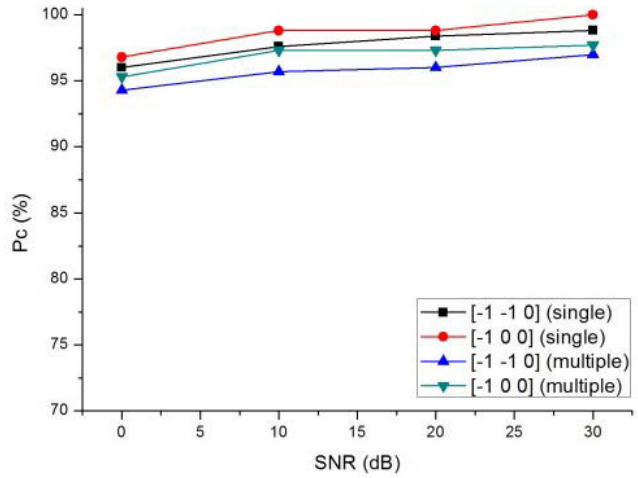

(b) Random targets

Figure 6. P_c versus SNR.

scenarios, $P_c >$ 93.7% for $N_g = 3$ ($N_t = 27$ and $N_t \times 5 = 135$ training images). This result proves that the ISAR image is insensitive to variation in the aspect angle. Therefore, classification of ISAR images requires only a small number of training images (21.6 % of $N_g = 5$) due to the stable 2D characteristics of the ISAR image.

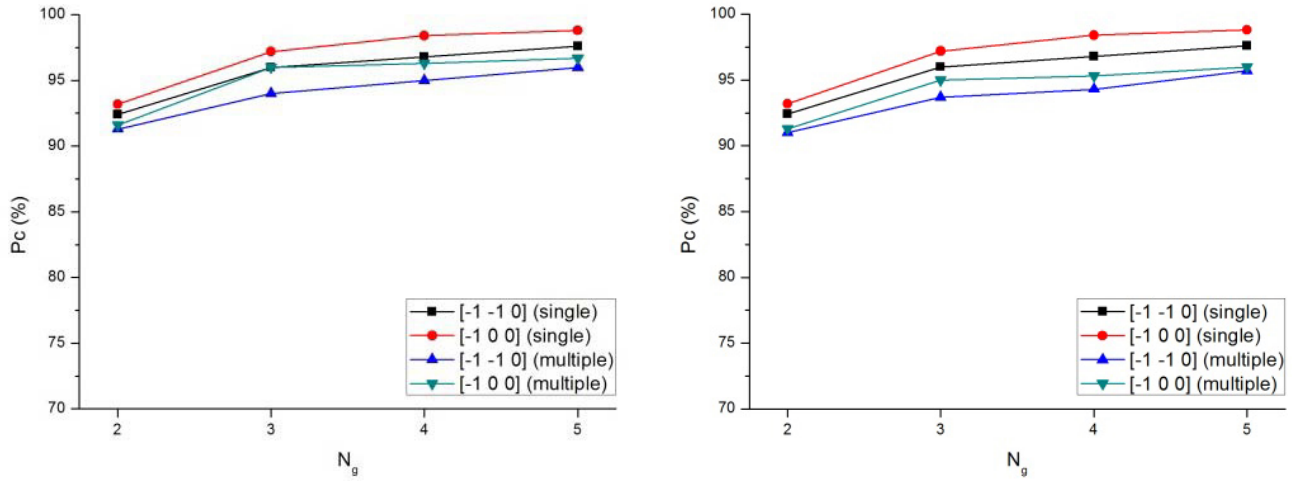

(a) Identical targets (b) Random targets

Figure 7. P_c versus number of grids per axis.

3.2. Simulation Results Using a Real Boeing 747 Aircraft

The segmented ISAR image of the real Boeing 747 aircraft was tested to demonstrate the effectiveness of the proposed method. After taking off at 1 km range (Fig. 8), the aircraft was observed for 17.75 s using a fixed X-band chirp radar with PRF = 2 kHz, B = 100 MHz (1.5-m resolution), and antenna beam width = 8.9°. Because the aircraft flew away from the radar, the 35500 RPs obtained were tilted, and had pulse numbers that increased with distance (Fig. 9(a)). To simulate ATR of five targets, the 35500 RPs were divided into five groups of 7100 RPs, and each group was assumed to be measured from a different target (Fig. 9(b)).

Figure 8. Observation scenario of the real Boeing 747.

Assuming that the aircraft speed was 60 m/s and that the cross-range resolution was equal to the down-range resolution = 1.5 m, the required angular variation for ISAR imaging was $\Delta\theta = 0.01$ rad and the corresponding flight length was to 16.39 m. As a result, the coherent processing time was set to $16.39/60 = 0.2732$ s, and the number of pulses (RPs) for ISAR imaging was set to $0.2732 \times 2000 = 546$. The training database was constructed by sampling ISAR images for every $N_p = 10$ RPs, yielding 656 training images per target. In the test phase, RPs of three randomly selected targets were placed so that the ISAR images did not overlap, then the obtained ISAR images were segmented, yielding 300 test images. The jet engine modulation by the rotating jet turbines was removed by applying the method of adaptive chirplet representation [18]. ISAR images obtained by using the segmentation algorithm were correctly segmented (Fig. 10).

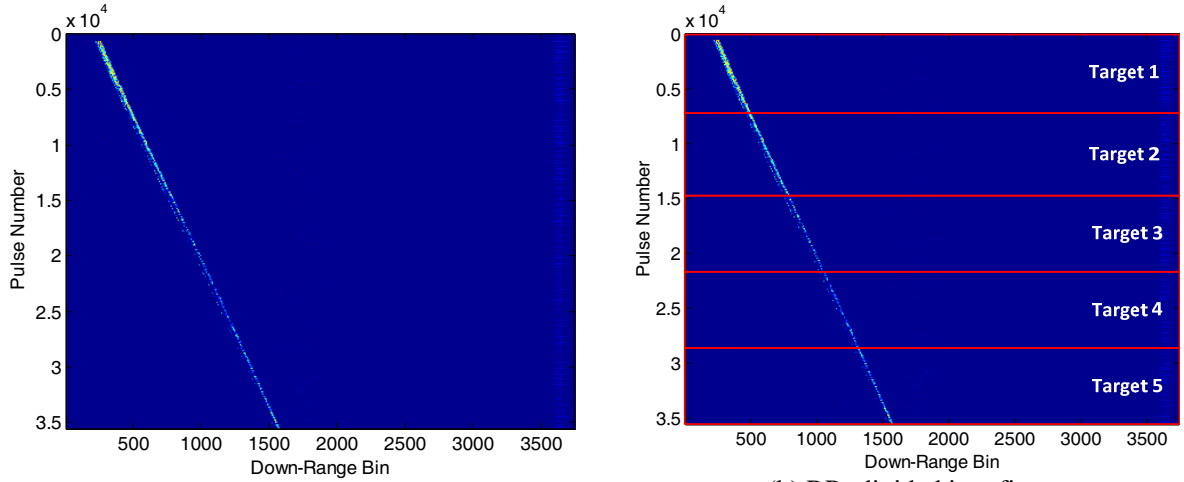

(a) RPs of Boeing 747 (b) RPs divided into five groups

Figure 9. Measured RPs of Boeing 747 and division into 5 targets.

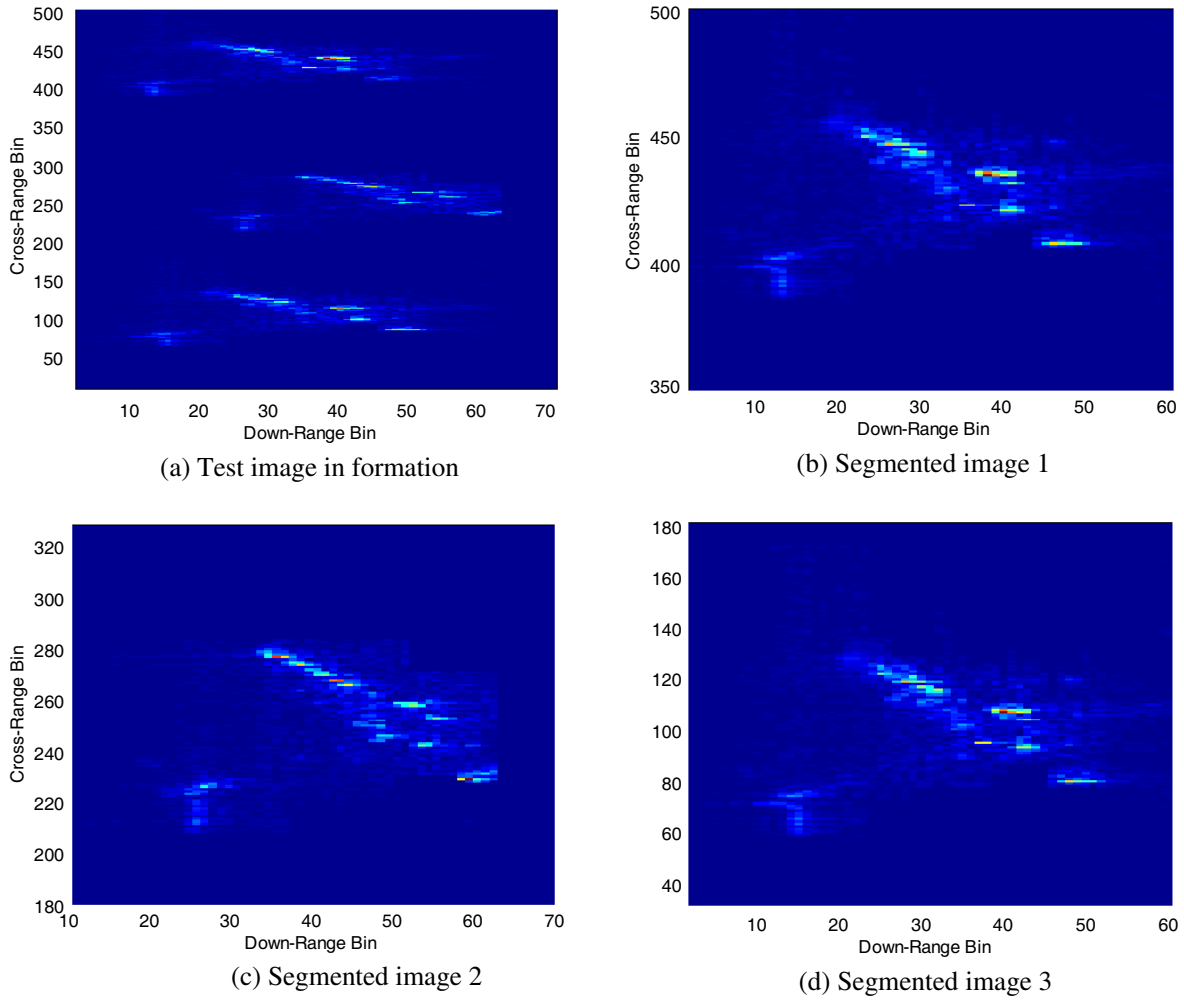

(a) Test image in formation (b) Segmented image 1

(c) Segmented image 2 (d) Segmented image 3

Figure 10. Test image in formation and segmented images.

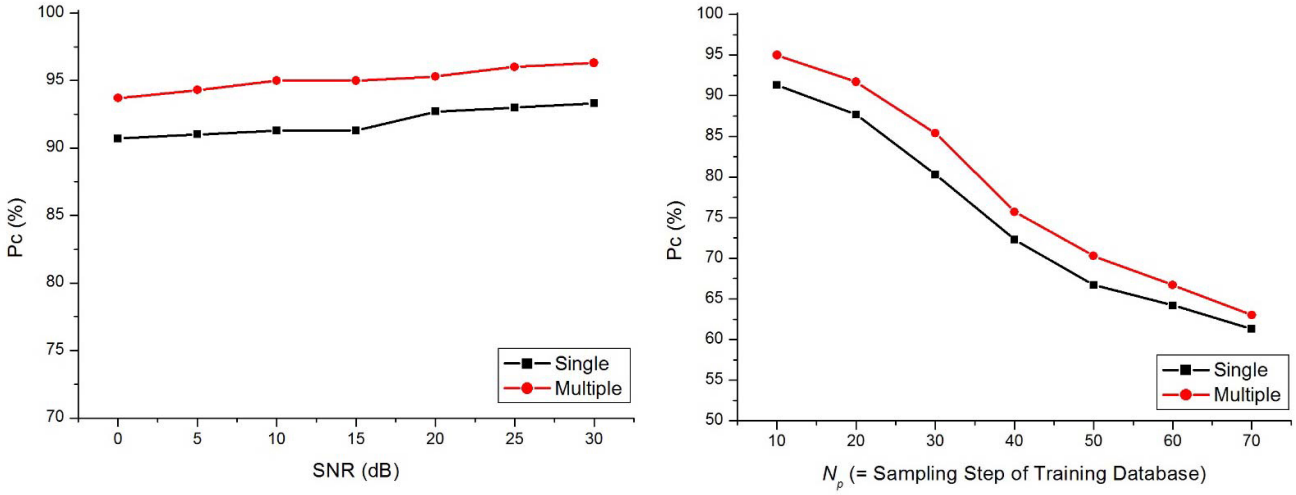

(a) P_c versus SNR (b) P_c versus N_p (SNR = 15 dB)

Figure 11. ATR result of the real Boeing 747.

The classification result by the proposed method was not significantly different from the single-target classification (Fig. 11). For various SNRs, P_cs were lower by only 2–3%, and those obtained for various N_ps were lower by 2–4%; this small degradation demonstrates the efficiency of the proposed method. Because of the robustness of coherent processing of ISAR imaging, P_c did not increase considerably for the increase of SNR. However, increase of N_p, i.e., decrease of the number of training images, yielded considerable degradation of accuracy; P_c of the formation flight decreased considerably from 91.3% to 61.3% and that of the solo flight decreased from 95% to 63%. This result demonstrates that successful ATR using ISAR images requires a training database of sufficient size.

4. CONCLUSION

We proposed an ATR procedure by fusing a method for segmentation of the ISAR image, a scenario-based construction method, and an efficient polar-mapping classifier. The proposed procedure was demonstrated by using segmented ISAR images derived from five targets composed of point SCs flying in formation and the measured data of a Boeing 747 aircraft. The overall ATR results prove that ISAR imaging is a very useful tool even when the reflected radar signal of each target is contaminated by reflections from neighboring targets. ATR results using the segmented ISAR for the formation flight of identical targets and randomly selected targets were not greatly degraded by noise or by decrease in the size of the training database. Compared with the single target classification in two flight scenarios, the amount of performance reduction was $< 3\%$ due to the negligible loss of information contained in the ISAR image. In the simulation using point SCs, P_cs obtained using the measured Boeing 747 data were very stable for various SNRs for both solo and formation flights and the result was considerably dependent on the N_p, i.e., the training database size. Therefore, for ATR to be successful, the training database size must be large enough. Compared with the solo flight, P_cs of the formation flight degraded by only $< 4\%$, this result demonstrates that the proposed method is appropriate for ATR of a real target.

ACKNOWLEDGMENT

This research was supported by Basic Science Research Program through the National Research Foundation of Korea (NRF) funded by the Ministry of Education, Science and Technology (2012R1A1A1002047).

REFERENCES

1. Park, S.-H., M.-G. Joo, and K.-T. Kim, "Construction of ISAR training database for automatic target recognition," *Journal of Electromagnetic Waves and Applications*, Vol. 25, Nos. 11–12, 1493–1503, 2011.
2. Park, J.-I. and K.-T, Kim, "A comparative study on ISAR imaging algorithms for radar target identification," *Progress In Electromagnetics Research*, Vol. 108, 155–175, 2010.
3. Choi, G.-G., S.-H. Park, H.-T. Kim, and K.-T. Kim, "ISAR imaging of multiple targets based on particle swarm optimization and Hough transform," *Journal of Electromagnetic Waves and Applications*, Vol. 23, Nos. 14–15, 1825–1834, 2009.
4. Park, S.-H., H.-T. Kim, and K.-T. Kim, "Enhanced range alignment using a combination of a polynomial and gaussian basis functions," *Progress In Electromagnetics Research*, Vol. 95, 381–396. 2009.
5. Park, S.-H., H.-T. Kim, and K.-T. Kim, "Stepped-frequency ISAR motion compensation using particle swarm optimization with an island model," *Progress In Electromagnetics Research*, Vol. 85, 25–37, 2008.
6. Park, S.-H., K.-K. Park, J.-H. Jung, H.-T. Kim, and K.-T. Kim, "Construction of training database based on high frequency RCS prediction methods for ATR," *Journal of Electromagnetic Waves and Applications*, Vol. 22, Nos. 5–6, 693–703, 2008.
7. Park, S.-H., K.-K. Park, J.-H. Jung, H.-T. Kim, and K.-T. Kim, "ISAR imaging of multiple targets using edge detection and Hough transform," *Journal of Electromagnetic Waves and Applications*, Vol. 22, Nos. 2–3, 365–373, 2008.
8. Menon, M. M., E. R. Boudreau, and P. J. Kolodzy, "An automatic ship classification system for ISAR imagery," *The MIT Lincoln Labaratory Journal*, Vol. 6, No. 2, 289–308, 1993.
9. Musman, S., D. Kerr, and C. Bachmann, "Automatic recognition of ISAR ship images," *IEEE Trans. Aerosp. Electron. Syst.*, Vol. 32, No. 4, 1392–1404, 1996.
10. Chen, C. C. and H. C. Andrews, "Target-motion-induced radar imaging," *IEEE Trans. Aerosp. Electron. Syst.*, Vol. 16, No. 1, 2–14, Jan. 1980.
11. Chen, V. C. and H. Ling, *Time-frequency Transforms for Radar Imaging and Signal Analysis*, Artech House, INC, 2002.
12. Jung, J.-H., K.-T. Kim, S.-H. Kim, and S.-H. Park, "An efficient ISAR imaging method for multiple targets," *Progress In Electromagnetics Research*, Vol. 146, 133–142, 2014.
13. Park, S.-H., H.-T. Kim, and K.-T. Kim, "Segmentation of ISAR images of targets moving in formation," *IEEE Trans. on Geoscience and Remote Sensing*, Vol. 48, No. 4, 2099–2108, Apr. 2010.
14. Park, J.-I. and K.-T. Kim, "A comparative study on ISAR imaging algorithms for radar target identification," *Progress In Electromagnetics Research*, Vol. 108, 155–175, 2010.
15. Li, W.-T., X.-W. Shi, and Y.-Q. Hei, "An improved particle swarm optimization algorithm for pattern synthesis of phased arrays," *Progress In Electromagnetics Research*, Vol. 82, 319–332, 2008.
16. Kim, K.-T., D.-K. Seo, and H.-T. Kim, "Efficient classification of ISAR images," *IEEE Trans. on Antennas and Propagation*, Vol. 53, No. 5, 1611–1621, May 2005.
17. Park, S.-H., "Automatic recognition of targets in formation using range profiles," *Journal of electromagnetic Waves and Applications*, Vol. 26, Nos. 14–15, 2059–2069, Oct. 2012.
18. Jung, J.-H., K.-T. Kim, and S.-H. Park, "Removal of JEM signal by accurate estimation of initial parameters of chirplet basis functions," *Progress In Electromagnetics Research*, Vol. 141, 607–618, 2013.